International Journal of Computational and Experimental Science and ENgineering (IJCESEN)

Vol. 11-No.4 (2025) pp. 10113-10121
http://www.ijcesen.com

ISSN: 2149-9144

Research Article

Comparison of Treatment Planning Systems with Monte Carlo Simulation Under Conditions of Tissue Inhomogeneities

Türkay Toklu[1,2]*, Bahar Dirican[3], Necdet Aslan[4]

[1]Department of Physics, Yeditepe University, Inonu Mh. Kayisdagi Cd. 26 Agustos Yerlesimi, Atasehir, Istanbul-Turkiye
[2]Yeditepe University Hospital, Department of Nuclear Medicine, Kosuyolu Mh. Kosuyolu Cd. No:128 Kadikoy, Istanbul-Turkiye
* **Corresponding Author Email:** toklu@yeditepe.edu.tr - **ORCID:** 0000-0002-5399-9394

[3]Gülhane Education and Research Hospital, Radiation Oncology Department, 06010, Ankara-Turkiye
Email: diricanbahar@gmail.com - **ORCID:** 0000-0002-1749-5375

[4]Department of Physics, Yeditepe University, Inonu Mh. Kayisdagi Cd. 26 Agustos Yerlesimi, Atasehir, Istanbul-Turkiye
Email: naslan@yeditepe.edu.tr - **ORCID:** 0000-0001-8766-1132

Article Info:

DOI: 10.22399/ijcesen.4006
Received : 01 September 2025
Revised : 11 November 2025
Accepted : 28 December 2025

Keywords:

Monte Carlo simulation,
EGSnrc/BEAMnrc code,
Treatment Planning Systems,
Tissue Inhomogeneities,
Slab phantom.

Abstract:

This study aimed to validate a Monte Carlo (MC) beam model of a 6-MV Elekta Synergy MLCi linac and benchmark tests of two different treatment planning systems (TPSs) employing pencil-beam (PB) and collapsed-cone convolution/superposition (CCC) algorithms against MC in heterogeneous slab phantoms. The initial electron energy was optimized by χ^2 analysis of water-phantom PDDs and lateral profiles for field size of 10×10 cm^2 (5.4–6.6 MeV); 5.8 MeV minimized χ^2 and was adopted. Agreement with measurement was verified using percent depth dose curves, lateral dose profiles, $TPR_{20,10}$ and output factors. Dose distributions of 3×3, 10×10 and 20×20 cm^2 open fields in lung-, bone- and water-equivalent virtual slab phantoms were then calculated using both TPSs and MC method. MC calculations were performed in two modes: one yielding dose-to-medium (MC_{Dm}) and the other yielding dose-to-water (MC_{Dw}). At 5.8 MeV, measurements versus MC comparisons showed <0.5% differences for PDDs (≤20×20 cm²), ~1% for lateral profiles (outside high-gradient regions), $TPR_{20,10}$ <0.2% and ~1% for output factors. In the lung phantom and 3×3 cm^2 field, PDD differences of up to 10% were observed between TPS_{PB} and MC_{Dw}, whereas the corresponding difference for TPS_{CCC} was 4.5%. The differences were smaller in the other phantoms. In the dose profile comparisons, particularly at the field edges, discrepancies of up to 14% were observed. In conclusion, the MC model demonstrated a high level of agreement with measurements. TPS_{CCC} calculations were closer to those by MC_{Dw} than TPS_{PB}.

1. Introduction

Accurate dose calculations are essential for the quality of radiotherapy treatment planning and therefore doses delivered to patient [1,2]. In the last few decades, the sophistication and the level of refinement of the dose calculation models implemented in clinical radiotherapy treatment planning systems have increased gradually [3,4]. It is well accepted that Monte Carlo (MC) methods offer the most powerful tool for modelling radiation transport in the human body for radiotherapy applications [5].

MC based treatment planning and plan verification have been widely used at radiotherapy departments all around the world. Accuracy of these tasks strongly depend on success of the simulation. For a successful MC simulation, not only the technical information about the linac, but also the determination of initial electron beam characteristics, which is optimized at the installation of the linac, are important. Accurate measurements of various parameters are necessary for comparisons with MC results.

Conventional clinical treatment planning systems (TPSs), such as pencil- beam (PB) and collapsed-cone convolution/superposition (CCC) algorithms, approximate radiation transport using parameterizations that are calibrated to reference conditions and largely report dose as dose-to-water

(Dw). By contrast, MC methods model particle transport explicitly and, when materials are assigned with their elemental composition, naturally compute dose-to-medium (Dm) in each voxel. As emphasized by the AAPM Task Group 105 (Chetty et al., 2007) [1], MC's material- true description yields Dm by construction, whereas most clinical commissioning data, reference protocols, and prescription practices are historically aligned with Dw.

The conceptual and practical implications of this mismatch have been discussed extensively. Using cavity theory, Dm may be converted to Dw via mass collisional stopping- power ratios and, where applicable, fluence corrections. Siebers et al. (2000) [6] showed that these Dm→Dw corrections are typically small in soft tissue (often within a few percent), but can become non-negligible in high-Z media such as cortical bone, approaching ~5–10% depending on beam quality and composition.

In this study, an Elekta Synergy MLCi linear accelerator was modelled using MC simulation, and dose distributions generated in virtual phantoms incorporating tissue inhomogeneities were compared against those from two clinical TPSs commissioned for the same linac and employing two distinct calculation algorithms. To enable a direct comparison with TPS outputs, a second set of MC calculations was performed in phantoms composed solely of water but assigned with different physical (and thus electron) densities.

2. Material and Methods

2.1. Monte Carlo model of the linac

The Monte Carlo model of the 6-MV photon beam of the Elekta Synergy MLCi linac (Elekta Oncology Systems, Crawley, UK) installed at Gülhane Education and Research Hospital, Department of Radiation Oncology was modelled by taking into consideration of the technical specifications provided by the manufacturer. The 2010 version of EGSnrc/BEAMnrc Monte Carlo code system [7,8] used in the study. Tungsten target, tungsten-rhenium alloy primary collimator, steel flattening filter with aluminum carrier, ionization chamber and aluminum back-scatter plate were simulated using SLABS, CONS3R, FLATFILT, SLABS, CHAMBER and SLABS component modules (CMs), respectively (Figure 1).

Curved-end multi-leaf collimators (MLCs) were simulated using MLCE CM. The leaves with tongue-and-groove arrangement are made from tungsten alloy and have a radius of 15 cm. The X back-up jaws (3 cm thick), which have also curved-end with a radius of 7 cm, were simulated with MLCQ CM. Y-jaws (made from tungsten alloy) were simulated using JAWS CM. Following mylar crosswire sheet, a 1 mm thick air slab at 70 cm from the target was placed for all the simulations to produce Phase-Space (PhSp) files that were used as source in DOSXYZnrc code for phantom simulations [9].

The photon and the electron cut-off energies were set to 10 and 700 keV, respectively. Variance reduction techniques including directional Bremsstrahlung splitting, electron splitting at flattening filter and range rejection with constant cut-off energy of 2 MeV were used in both BEAMnrc and DOSXYZnrc codes [10].

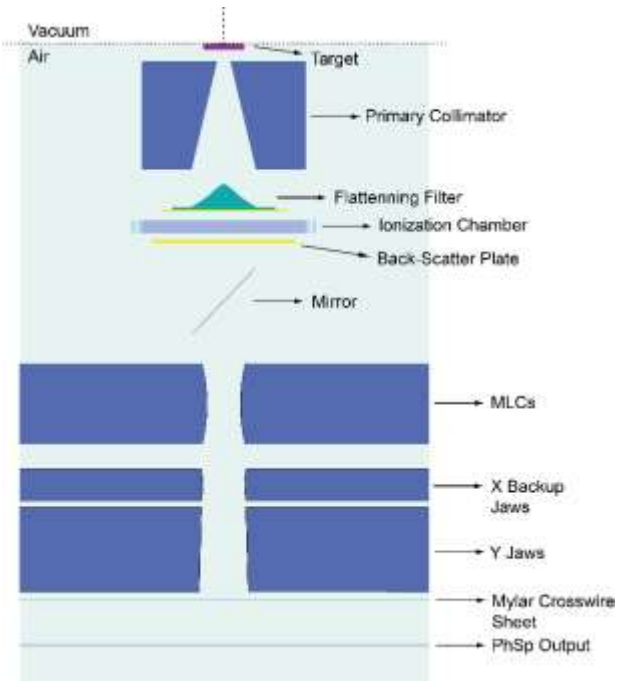

Figure 1. *Monte Carlo simulation view of Elekta Synergy MLCi treatment head. Mirror and Y-jaws were rotated 90° around central axis (CAX) to be visualized.*

2.2. Measurements

Percent depth dose (PDD) curves and dose profiles were measured using IBA Blue Water Phantom with IBA CC13 0.13 cm^3 ionization chamber (IBA dosimetry, Schwarzenbruck, Germany). PDD curves were measured for open fields from 3×3 cm^2 to 40×40 cm^2. The dose profiles at 10 and 20 cm depths were also measured for 3×3, 10×10 and 20×20 cm^2 open fields. All the profiles were measured in the direction perpendicular to the direction of MLCs' motion. PDD curves and profiles were obtained with OmniPro-Accept software (IBA dosimetry, Schwarzenbruck, Germany), a part of IBA Blue Water Phantom.

Water equivalent solid phantoms composed of RW3 material (PTW Freiburg, Freiburg, Germany) and IBA FC65-P 0.65 cm^3 ionization chamber (IBA dosimetry, Schwarzenbruck, Germany) were used

for $TPR_{20,10}$ and output measurements. Outputs were measured at 5 cm depth from the surface and expressed at d_{max} using PDD curves for each field size.

2.3. Validation of Monte Carlo simulation

For the determination of the incident electron beam parameters, we varied only the mean initial electron energy, while keeping both the radial intensity profile and the energy spread fixed [11]. A circular electron source was implemented in BEAMnrc (source 19) with a Gaussian radial profile (Full-Width at Half Maximum, FWHM = 1 mm in X and Y directions) and a Gaussian energy distribution (FWHM = 1 MeV) [12]. To determine the appropriate initial electron mean energy, electron beams with mean energy from 5.4 to 6.6 MeV were selected with 0.2 MeV increments. SSD was chosen to be 100 cm, field size was set to 10×10 cm^2, and the number of initial electrons was chosen to be 10^8 for each simulation. PhSp files 70 cm from the target were created after each simulation using BEAMnrc. In order to obtain 3-dimensional dose distribution in water, a 40×40×40 cm^3 water phantom with voxel size of 0.2×0.2×0.2 cm^3 created in DOSXYZnrc. PhSp files created in BEAMnrc were used as initial particles (electrons, positrons and photons) in DOSXYZnrc via source number 2 of DOSXYZnrc. Following MC calculations, three-dimensional dose outputs of DOSXYZnrc were ingested via the DICOM-RT toolbox [13] embedded in Computational Environment for Radiotherapy Research (CERR version 4.0beta2), developed at Washington University, St. Louis [14]. PDD curves and dose profiles were extracted from these files in MATLAB version 7.6 (The MathWorks, Inc., Natick, MA, USA).
For 10x10 cm^2 open field and SSD=100 cm, PDD curves and dose profiles for each electron beam energy were compared with χ^2 analysis. The mean energy value that minimizes χ^2 was selected as the most appropriate value for initial energy of the electron beam. At this energy, PDD curves and dose profiles for open field sizes other than 10×10 cm^2 were compared with ionization chamber measurements. Sufficient initial number of electrons (10^8 to 5×10^8) depending on the field size was used to keep statistical uncertainty under 0.5%. The beam quality parameter, $TPR_{20,10}$ was also evaluated.
Output factor measurements were simulated using a 0.5×0.5×0.2 cm^3 sized single voxel at 5 cm depth of water. The voxel was designed to be surrounded by 20 cm thick rectangular water from each side and the bottom.

2.4. Slab phantoms

Three virtual layered phantoms shown in Figure 2 were created using MATLAB in the form of 3D matrix with dimensions of 512×512×121 voxels [15]. Matrices were then converted to computed tomography (CT) images with the CERR and exported as DICOM images.

2.5. Treatment planning systems

Two treatment planning systems (TPSs) with different dose calculation algorithms were compared with MC calculated dose distributions. PrecisePLAN v2.10 (Elekta Oncology Systems, Crawley, UK) utilizes Pencil Beam (PB) algorithm with tissue inhomogeneity correction algorithm of TAR Ratio Method, Pinnacle3 v8.0 (Philips Medical Systems, Andover, MA) uses 3D Adaptive Collapse Cone Convolution-Superposition (CCC) algorithm for calculation patient dose distributions. The TPSs were named by the aberrations of TPS_{PB} and TPS_{CCC}, respectively. Both TPSs were commissioned according to the acceptance criteria by

Figure 2. a) *Construction of the virtual layered CT phantoms. For each phantom material labelled as [1] is water with CT number of 1000 and material labelled as [3] is air with CT number of 0.* ***b)*** *Lung phantom viewed in a standard lung window. Material [2] presents lungs with CT number of 175, which is derived from CT images of 5 patients with regular breathing.* ***c)*** *Bone phantom viewed in a standard abdomen window. Material [2] presents cortical bone with CT number of 2000. The third phantom just consists of water with CT number of 1000.*

Van Dyk et al. [16] with the same set of PDD and dose profile measurements.

The third order polynomial function defined for Hounsfield Unit (HU) to relative electron density conversion in TPS_{PB} was selected as reference conversion table (Figure 3.a). For TPS_{CCC}, however, physical density values were used instead of relative electron density. Additionally, the conversion must be defined by a set of linear equations instead of a third-order polynomial. To achieve this, HU to relative electron density conversion function of TPS_{PB} was represented with a set of linear equations (Figure 3.b). A bi-linear transformation was generated from physical densities and corresponding relative electron densities of materials in the Gammex Model 467 and CIRS Model 062M phantoms; this calibration was subsequently used to convert relative electron density to physical density in our datasets [15].

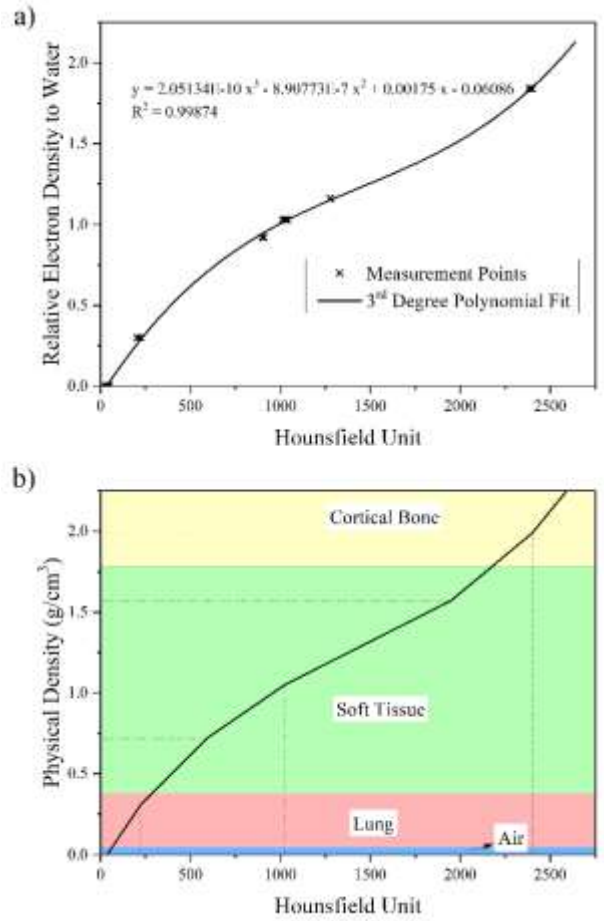

Figure 3. a) *Hounsfield Unit to relative electron density conversion for* TPS_{PB}. ***b)*** *Hounsfield Unit to physical density conversion for* TPS_{CCC} *and* MC_{Dm}.

2.6. HU to physical density conversions in MC

In this study, two different HU to physical density conversions were used in MC calculations. In the first approach, the materials and tissues (air, lung tissue, soft tissue, cortical bone) together with their corresponding physical density values, as reported by Kawrakow et al. (1996) [17], were used (Figure 3b). The dose distribution obtained with this conversion was denoted as MC_{Dm} (dose-to-medium). In the second approach, all materials were assumed to be water, and the resulting dose distribution was denoted as MC_{Dw} (dose-to-water). In both conversions, the same set of linear equations employed in TPS_{CCC} was applied.

2.7. Dose calculations in slab phantoms

All phantoms were planned in both TPSs for beams directed to -y direction with field sizes of 3×3, 10×10 and 20×20 cm^2 and SSD=100 cm. Dose grid was 0.2×0.2×0.2 cm^3.

The same plans were simulated with MC. PhSp files generated to validate simulation were used as initial particles in DOSXYZnrc via source number 2 of DOSXYZnrc. CT images of slab phantoms were converted to DOSXYZnrc phantom files using CTCREATE tool [18] with two different HU conversion methods stated above. Statistical uncertainty for each simulation was less than 0.5%.

All dose distributions and plan details exported from TPSs via DICOM-RT format as well as dose output files from MC simulations were imported within CERR. PDDs along the CAX and dose profiles at 4.5 cm depth (in the middle of the inhomogeneity insert of the phantoms) were obtained in MATLAB. Penumbra width between 80% and 20% of dose at CAX were also calculated for each distribution.

3. Results and Discussions

3.1. Simulation validation

The χ^2 values obtained from comparison of ionization chamber measurements and MC simulations in terms of PDD curves and dose profiles of 10×10 cm^2 open field for each selected electron beam energy are given in Table 1.

The mean electron beam energy of 5.8 MeV that minimizes the χ^2 was selected as the initial electron beam energy and used in all further simulations. At this energy, an excellent correlation was observed between measured and calculated $TPR_{20,10}$ values an identifier for beam quality (0.678 vs 0.679). The difference was less than 0.2%. This minor difference indicates that the energy spectra of the photon beams from the linac and from the simulation are in close agreement.

The comparison of the selected PDD and dose profile curves is given in Figure 4.a-b. Less than 0.5% differences were obtained in PDD comparisons between MC simulation and ionization chamber

measurements for field sizes of 20×20 cm^2 and smaller. As for dose profile comparisons, differences between MC simulations and measurements were within 1.0% except for the penumbra regions.

Table 1. *χ^2 values against initial electron beam energy.*

Initial Electron Beam Energy (MeV)	χ^2 values		
	PDD curve	Dose Profile @ 10 cm depth	Dose Profile @ 20 cm depth
5.4	0.348	0.208	0.282
5.6	0.117	0.184	0.160
5.8	**0.033**	**0.079**	**0.049**
6.0	0.206	0.100	0.158
6.2	0.574	0.151	0.347
6.4	1.146	0.483	0.835
6.6	1.784	0.595	1.195

In the penumbral regions of the lateral profiles, we observed dose differences of up to 8% between Monte Carlo (MC) calculations and ionization chamber measurements. Such discrepancies are expected in steep lateral dose gradients and are largely attributable to volume-averaging effects associated with the relatively large sensitive volume of ionization chambers. Consistent with our observations, Haryanto et al. (2002) [19] compared profiles measured with multiple detector types against MC simulations and reported agreement within 2% for diamond and silicon diode detectors, while the largest deviations occurred when using ionization chambers specifically in the penumbra. They concluded that the chamber's finite sensitive volume was the principal cause of the observed smoothing and under/over-response in high-gradient regions. Similar findings have been reported by other investigators [20,21].

Across all open field sizes, discrepancies between calculated output factors and ionization-chamber measurements were lower than 1.0% (Figure 4.c).

After optimizing the mean initial electron beam energy, the Monte Carlo (MC) model showed close agreement with ionization chamber measurements across the PDD curves, dose profiles, and output factors. This consistency supports the model's suitability for heterogeneous slab-phantom investigations, and it was used as a reliable benchmark for the verification and quality assurance of treatment-planning algorithms.

3.2. Phantom dose distributions

Dose distributions calculated by MC_{Dm} for Lung Phantom for different field sizes are given in Figure 5.a-c. PDD curves from TPSs and MC calculations for all phantoms and all field sizes are shown in Figure 5.d-l.

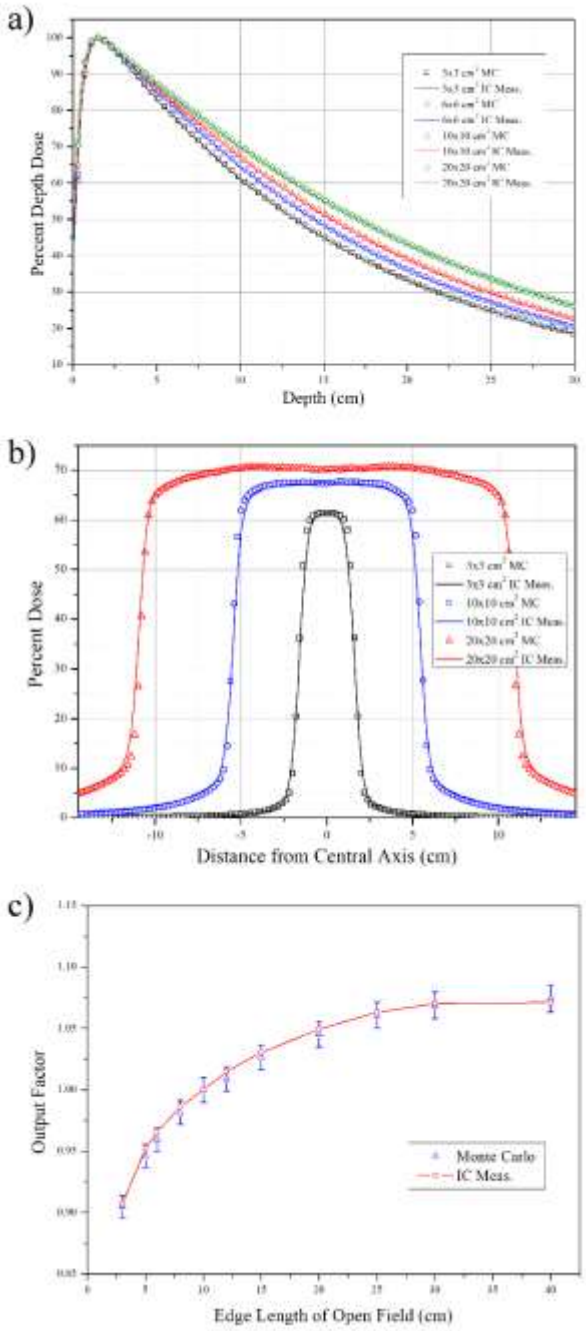

Figure 4. *Comparison plots of Monte Carlo (MC) and Ionization Chamber (IC) measurements in terms of* ***a)*** *PDDs* ***b)*** *dose profiles at 10 cm depth and* ***c)*** *output factors.*

In Lung Phantom, for 3×3 cm^2 open field, a rapid dose drop was observed for all calculation methods except for TPS_{PB}. This expected behavior is mainly due to lateral electronic disequilibrium in small field sizes [22-24]. This effect was not observed for larger field sizes where lateral electronic equilibrium was fulfilled. Dose difference was 8% between TPS_{PB} and MC_{Dw} at 4.5 cm depth for 3×3 cm^2 open field.

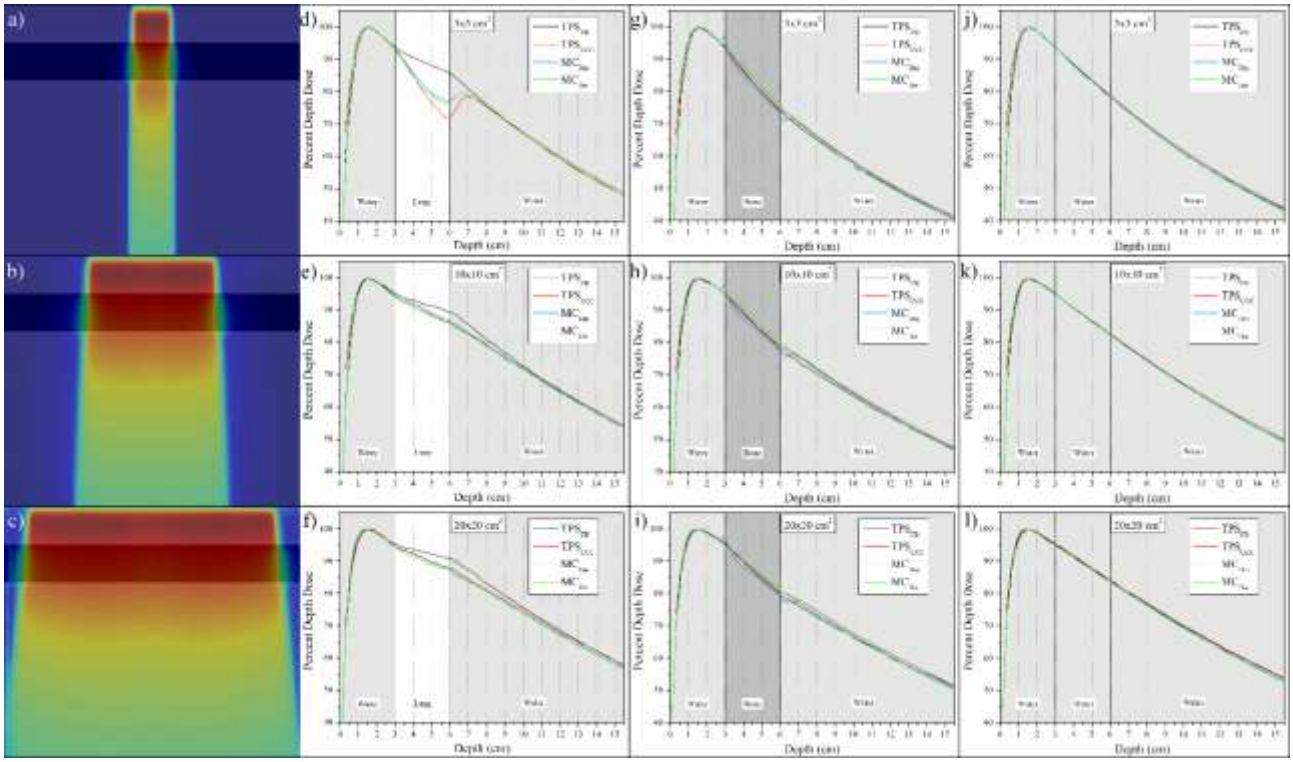

Figure 5. *Dose distributions calculated by MC_{Dm} for Lung Phantom for 3×3, 10×10 and 20×20 cm^2 field sizes* ***(a-c)****. Corresponding PDD curves along CAX for Lung Phantom* ***(d-f)****, Bone Phantom* ***(g-i)*** *and Water Phantom* ***(j-l)****.*

This value is 2.5% for 10×10 cm^2 and 20×20 cm^2 fields. The difference increases as the depth increases up to 10% for 3×3 cm^2 and to 3.5% for 10×10 cm^2 and 20×20 cm^2 open fields. The difference between TPS_{CCC} and MC_{Dw} was 1.0% at 4.5 cm depth for 3×3 cm^2 open field. Again, the difference increased as depth increases up to 4.5%. The differences were 0.6% and 0.8% for 10×10 cm^2 and 20×20 cm^2 open fields, respectively. Up to 1.3% difference was observed between MC_{Dm} and MC_{Dw}. In their study, Carrasco et al. (2004) [25] had very similar results with other treatment planning systems that use PB and CCC calculation algorithms in comparison with Monte Carlo calculations using PENELOPE MC code. They have found that the CCC calculation algorithm showed good correlation with the MC calculation. The PDD curve they obtained with the PB algorithm was similar to those that was found in this study.

As for bone phantom, the dose differences between MC_{Dw} and both TPSs was lower than 2.0%, while the difference between TPSs was lower than 1.0% in inhomogeneity area for all field sizes. The dose difference between MC_{Dw} and MC_{Dm} was up to 3.0% in bone region. The main difference between these two calculation methods is the atomic composition of the medium. In MC_{Dw} calculation, all the atoms were composed of hydrogen and oxygen atoms. On the other hand, in MC_{Dm} calculation, the bone region was composed of hydrogen, carbon, nitrogen, oxygen, magnesium, phosphor, sulfur, calcium, and zinc atoms. Specifically, the presence of high-atomic-number elements modifies photon and electron transport parameters, leading to discrepancies between the two calculation approaches. In addition, the elevated electron density in bone region produced localized regions of abrupt dose increase and decrease. This effect was not observed in the MC_{Dw} results.

The percent dose difference between MC_{Dw} and both TPSs as well as MC_{Dm} calculations were less than 0.5% for three field sizes in water phantom. Since all calculation methods evaluated dose distributions in water, large dose discrepancies were not predicted.

Dose profiles at 4.5 cm depth (in the middle of tissue inhomogeneity region) from TPSs and MC calculations for all phantoms and all field sizes are presented in Figure 6.

For the lung phantom, when comparing dose profiles at a depth of 4.5 cm, particularly for the 3×3 cm^2 field size, TPS_{PB} yields higher percent doses than the other calculation algorithms. This finding is correlated with the PDD curves. For the remaining field sizes, the differences are smaller for in-field regions; however, at the field edges before penumbra region, TPS_{PB} calculates doses up to 5% higher, whereas TPS_{CCC} calculates doses up to 3% lower relative to MC_{Dw}.

In the bone phantom comparison, no substantial in-field dose differences were observed across all field sizes. At the field edges, however, TPS_{PB} exhibited deviations of up to 14% and TPS_{CCC} up to 8%

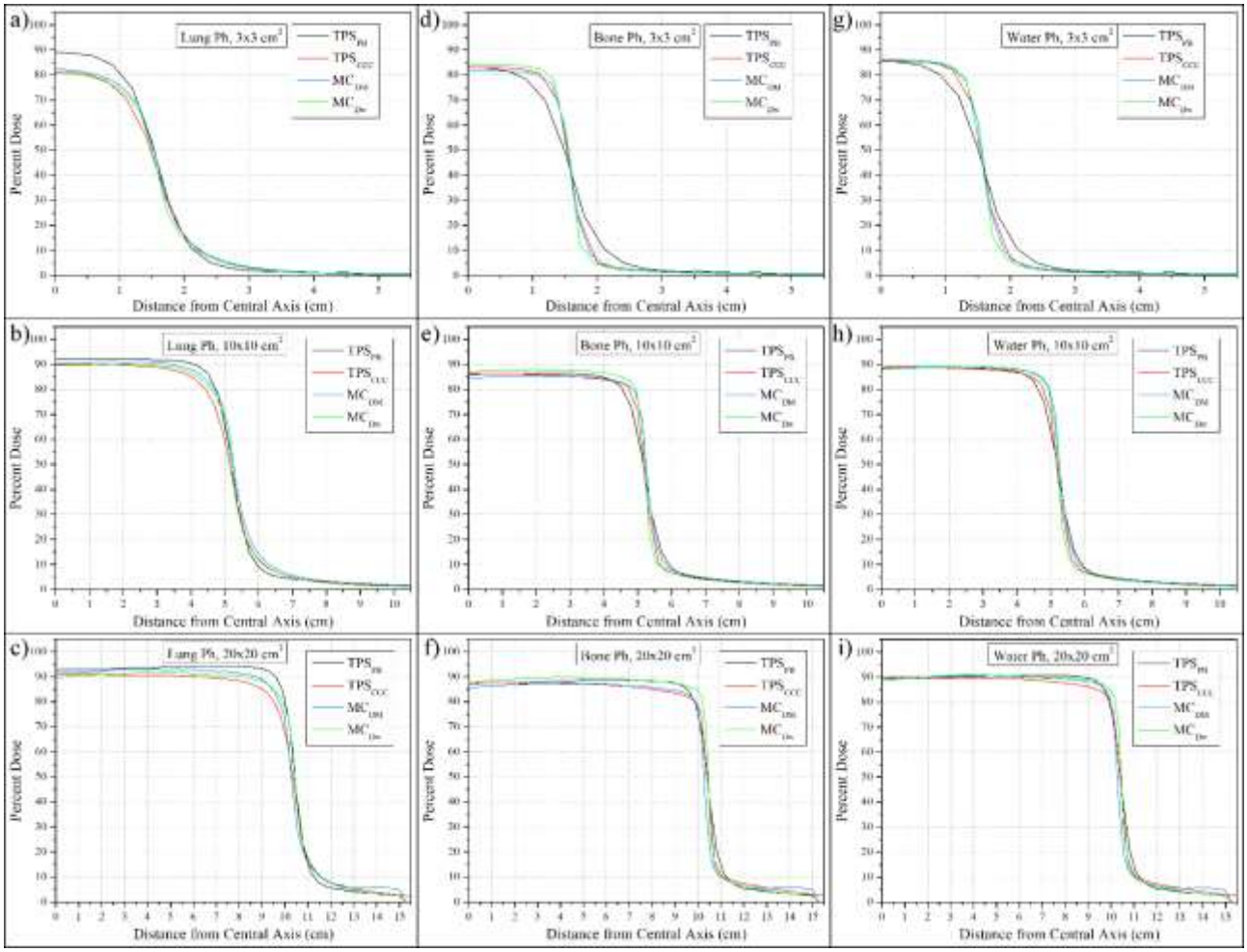

Figure 6. *Dose profiles at 4.5 cm depth for Lung Phantom* ***(a-c)****, Bone Phantom* ***(d-f)*** *and Water Phantom* ***(g-i)****. For clarity, only one half of each profile is shown.*

relative to the MC_{Dw} calculation for the 20 × 20 cm^2 field. In the water phantom comparison, discrepancies analogous to those observed in the bone phantom were also noted.

The penumbra widths (80%-20%) derived from the dose profiles are presented in Figure 7. As expected, all calculation methods showed an increase in penumbra width with increasing field size. Except for TPS_{PB}, the penumbra widths measured in the lung phantom are greater than those in the other phantoms. This behavior is expected due to enhanced lateral electron scattering in low-density lung tissue; however, TPS_{PB} algorithm did not disclose such density effect. The measurement of similar penumbra values in the other phantoms further supports this finding.

Higher penumbra widths in lung phantom were measured from TPS_{CCC} calculations in comparison with MC_{Dw} calculations. Similar behavior was observed for the other phantoms as well. Although TPS_{CCC} can account for material heterogeneities, it nonetheless overestimates the penumbra width relative to Monte Carlo calculations.

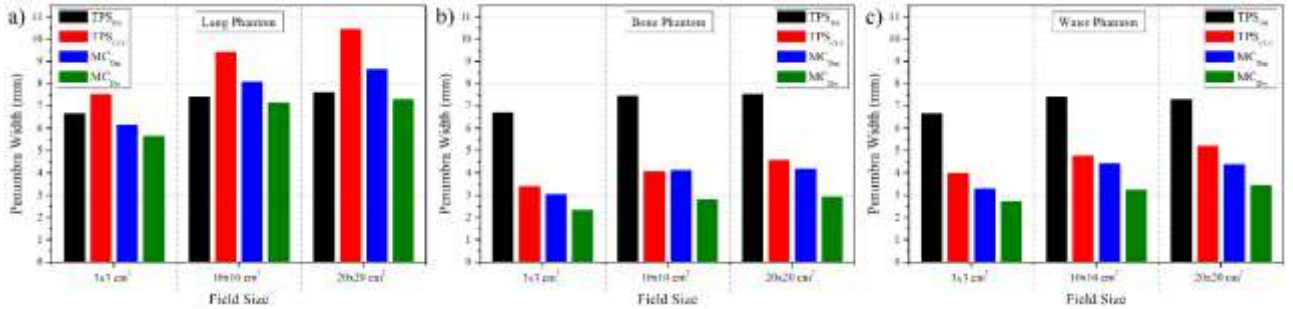

Figure 7. *Penumbra widths for* ***a)*** *Lung Phantom,* ***b)*** *Bone Phantom and* ***c)*** *Water Phantom.*

4. Conclusions

Within the scope of this study, the MC model demonstrated a high level of agreement with ion-chamber measurements across PDDs, profiles, and output factors. In heterogeneous slabs, TPS_{PB} shows systematic deviations in low-density lung tissue, most pronounced for small fields. Results were relatively better for bone and water phantoms. TPS_{CCC} generally aligns closely with MC across phantoms and field sizes, although it overestimates the lateral electron scattering.

Author Statements:

- **Ethical approval:** The conducted research is not related to either human or animal use.
- **Conflict of interest:** The authors declare that they have no known competing financial interests or personal relationships that could have appeared to influence the work reported in this paper
- **Acknowledgement:** The authors declare that they have nobody or no-company to acknowledge.
- **Author contributions:** The authors declare that they have equal rights on this paper.
- **Funding information:** The authors declare that there is no funding to be acknowledged.
- **Data availability statement:** The data that supports the findings of this study are available on request from the corresponding author. The data is not publicly available due to privacy or ethical restrictions.

References

[1] Chetty, I. J., Curran, B., Cygler, J. E., DeMarco, J. J., Ezzell, G., Faddegon, B. A., et al. (2007). Report of the AAPM Task Group No. 105: Issues associated with clinical implementation of Monte Carlo-based photon and electron external beam treatment planning. *Medical Physics*, 34(12):4818–4853.

[2] Ma, C.-M., Mok, E., Kapur, A., Pawlicki, T., Findley, D., Brain, S., et al. (1999). Clinical implementation of a Monte Carlo treatment planning system. *Medical Physics*, 26(10):2133–2143.

[3] Reynaert, N., Van der Marck, S. C., Schaart, D. R., Van der Zee, W., Van Vliet-Vroegindeweij, C., Tomsej, M., et al. (2007). Monte Carlo treatment planning for photon and electron beams. *Radiation Physics and Chemistry*, 76(4):643–686.

[4] Vanderstraeten, B., Reynaert, N., Paelinck, L., Madani, I., De Wagter, C., De Gersem, W., et al. (2006). Accuracy of patient dose calculation for lung IMRT: A comparison of Monte Carlo, convolution/superposition, and pencil beam computations. *Medical Physics*, 33(9):3149–3158.

[5] Verhaegen, F., & Seuntjens, J. (2003). Monte Carlo modelling of external radiotherapy photon beams. *Physics in Medicine and Biology*, 48(21):R107–R164.

[6] Siebers, J. V., Keall, P. J., Nahum, A. E., & Mohan, R. (2000). Converting absorbed dose to medium to absorbed dose to water for Monte Carlo based photon beam dose calculations. *Physics in Medicine and Biology*, 45(4):983–995.

[7] Rogers, D. W. O., Faddegon, B. A., Ding, G. X., Ma, C.-M., We, J., & Mackie, T. R. (1995). BEAM: A Monte Carlo code to simulate radiotherapy treatment units. *Medical Physics*, 22(5):503–524.

[8] Kawrakow, I. (2000). Accurate condensed history Monte Carlo simulation of electron transport: I. EGSnrc, the new EGS4 version. *Medical Physics*, 27(3):485–498.

[9] Kawrakow, I., & Walters, B. R. B. (2006). Efficient photon beam dose calculations using DOSXYZnrc with BEAMnrc. *Medical Physics*, 33(8):3046–3056.

[10] Kawrakow, I., Rogers, D. W. O., & Walters, B. R. B. (2004). Large efficiency improvements in BEAMnrc using directional bremsstrahlung splitting. *Medical Physics*, 31(10):2883–2898.

[11] Sheikh-Bagheri, D., & Rogers, D. W. O. (2002). Sensitivity of megavoltage photon beam Monte Carlo simulations to electron beam and other parameters. *Medical Physics*, 29(3):379–390.

[12] Rogers, D. W. O., Walters, B. R. B., & Kawrakow, I. (2009). *BEAMnrc user's manual (NRCC Report PIRS-509(A) revL).* National Research Council of Canada.

[13] Spezi, E., Lewis, D. G., & Smith, C. W. (2002). A DICOM-RT-based toolbox for the evaluation and verification of radiotherapy plans. *Physics in Medicine and Biology*, 47(21):4223–4232.

[14] Deasy, J. O., Blanco, A. I., & Clark, V. H. (2003). CERR: A computational environment for radiotherapy research. *Medical Physics*, 30(5):979–985.

[15] Toklu, T. (2016). *Use of Monte Carlo techniques in external beam therapy of lung cancer* [Doctoral dissertation, Yeditepe University]. Yeditepe University Library.

[16] Van Dyk, J., Barnett, R. B., Cygler, J. E., & Shragge, P. C. (1993). Commissioning and quality assurance of treatment planning computers. *International Journal of Radiation Oncology Biology Physics*, 26(2):261–273.

[17] Kawrakow, I., Fippel, M., & Friedrich, K. (1996). 3D electron dose calculation using a voxel based Monte Carlo algorithm (VMC). *Medical Physics*, 23(4):445–457.

[18] Walters, B. R. B., Kawrakow, I., & Rogers, D. W. O. (2009). *DOSXYZnrc user's manual (Report No. PIRS-794 RevB).* National Research Council of Canada.

[19] Haryanto, F., Fippel, M., Laub, W., Dohm, O., & Nüsslin, F. (2002). Investigation of photon beam output factors for conformal radiation therapy—Monte Carlo simulations and measurements. *Physics in Medicine and Biology*, 47(9):N133–N143.

[20] Scott, A. J., Nahum, A. E., & Fenwick, J. D. (2008). Using a Monte Carlo model to predict dosimetric properties of small radiotherapy photon fields. *Medical Physics*, 35(10):4671–4684.

[21] Heydarian, M., Hobany, P. W., & Beddoe, A. H. (1996). A comparison of dosimetry techniques in stereotactic radiosurgery. *Physics in Medicine and Biology*, 41(1):93–110.

[22] Disher, B., Hajdok, G., Gaede, S., & Battista, J. J. (2012). An in-depth Monte Carlo study of lateral electron disequilibrium for small fields in ultra-low density lung: Implications for modern radiation therapy. *Physics in Medicine and Biology*, 57(6):1543–1559.

[23] Fogliata, A., Vanetti, E., Albers, D., Brink, C., Clivio, A., Knöös, T., Nicolini, G., & Cozzi, L. (2007). On the dosimetric behaviour of photon dose calculation algorithms in the presence of simple geometric heterogeneities: Comparison with Monte Carlo calculations. *Physics in Medicine and Biology*, 52(5):1363–1385.

[24] Reynaert, N., Van der Marck, S. C., Schaart, D. R., Van der Zee, W., Van Vliet-Vroegindeweij, C., Tomsej, M., Jansen, J., Heijmen, B., Coghe, M., & De Wagter, C. (2007). Monte Carlo treatment planning for photon and electron beams. *Radiation Physics and Chemistry*, 76(4):643–686.

[25] Carrasco, P., Jornet, N., Duch, M. A., Weber, L., Ginjaume, M., Eudaldo, T., Jurado, D., Ruiz, A., & Ribas, M. (2004). Comparison of dose calculation algorithms in phantoms with lung equivalent heterogeneities under conditions of lateral electronic disequilibrium. *Medical Physics*, 31(11):2899–2911.